공학석사 학위논문

PSSA–*g*–PANI/Graphene Oxide Composite as a New Class of Hole Transport Layer for Enhanced Performance of Polymer Solar Cells

PSSA-*g*-PANI/Graphene Oxide 복합체의

유기태양전지 정공 수송 층으로의 적용과

효율 향상

2014년 2월

서울대학교 대학원

재료공학부

박 흥 수

Abstract

PSSA–*g*–PANI/Graphene Oxide Composite as a New Class of Hole Transport Layer for Enhanced Performance of Polymer Solar Cells

Park, Heung-su

Department of Materials Science and Engineering

Seoul National University

A new class of hole transport layer (HTL), which is composed of poly(styrene sulfonic acid) grafted with polyaniline (PSSA–*g*–PANI) and graphene oxide (GO), was prepared by adding GO into PSSA–*g*–PANI aqueous solution. The PSSA–*g*–PANI/GO composites exhibit high optical transparency and high electrical conductivity. When the composite with 2.5 wt% GO loading was used as HTL material for the device based on poly(3-hexylthiophene) and $PC_{61}BM$, the device exhibits an enhanced power conversion efficiency (PCE) of 4.23%, which is 23% higher than the PCE of device with the conventional HTL material, PEDOT:PSS. This enhancement of PCE arises mainly from an increase of the short-circuit current density due to higher optical transparency and higher electrical conductivity of PSSA–*g*–PANI/GO composite.

Keywords: PSSA–*g*–PANI, graphene oxide, hole transport layer, polymer solar cell

Student Number: 2012-20602

Contents

List of Schemes

List of Figures

List of Tables

Chapter 1. Introduction

Polymer solar cells (PSCs) undoubtedly have many advantages of low cost, ease of fabrication and the potentials for flexible, large area solar cells.[1] Remarkable improvements in the performance of PSCs have been achieved by introducing the donor-acceptor bulk heterojunction (BHJ) structure in the active layer.[2,3] Particularly, the BHJ polymer solar cells based on poly(3-hexylthiophene) (P3HT) and fullerene derivative phenyl-C61-butyric acid methyl ester ($PC_{61}BM$) have intensively been investigated, and huge amounts of experimental and theoretical data have been accumulated.[4–8] Recently, various low bandgap polymers that can absorb a broader range of the solar spectrum have been synthesized and high power conversion efficiencies (PCEs) were presented by using these polymers as active layer materials.[9,10] Compared to the active layer materials, however, few papers have reported the development of efficient hole transport materials to further enhance the photovoltaic performance of PSCs.[11,12]

The conventional PSC device is composed of four layers, indium tin oxide (ITO)/hole transport layer (HTL)/P3HT:$PC_{61}BM$/Al. In this BHJ solar cell structure, Poly(3,4-ethylenedioxythiophene):poly(styrenesulfonate) (PEDOT:PSS) has most widely been used as the hole transport layer material. HTL has been used in most of optoelectronic devices, because the introduction of HTL significantly improves both stability and performance of the devices by smoothing the ITO surface, lowering the work function of anode, and enhancing the hole transport.[13–16]

Although the performance of PSCs which use PEDOT:PSS as HTL has remarkably been progressed, various problems of PEDOT:PSS in the PSC device have been reported. First, since PEDOT:PSS is dispersed in water with large particle size with ca. 60–80 nm,[17] the aggregate of particles may play out as defects of the device, and therefore these defects would induce degradation of the PSC. Second, because of the strong acidic nature of PSS can lead to deterioration of solar cell performance, especially long-term stability and performance.[18] Third, PEDOT:PSS (CLEVIOSTM P VP AI 4081) has very high cost and low electrical conductivity (~10^{-3} S/cm).[19] Therefore, those problems become obstacles to achievement of highly efficient and large area PSCs. Consequently, there is a high demand to develop a new hole transport material, which is completely soluble in water (or various organic solvents) and shows better performance than PEDOT:PSS, to fabricate highly efficient and stable PSCs.

To resolve those problems, thin films of graphene oxide (GO)[20–22] and reduced GO[23,24] have recently been used as alternative HTL to PEDOT:PSS. GO, an oxidized derivative of graphene, is an attractive nanomaterial because of low cost, mass production and solution processability. GO is a graphene sheet functionalized with oxygen groups in the form of epoxy and hydroxyl group on the basal plane and various other types at the edges.[25–27] The C–O bonds are covalent and thus disrupt the sp^2 conjugation of the hexagonal graphene lattice, making GO an insulator. The electronic structure of GO is heterogeneous due to presence of mixed sp^2 and sp^3 hybridizations and therefore cannot be readily explained by traditional valence and

conduction band states.[28] Rather, lateral transport occurs by hopping between localized states (sp^2 sites) at the Fermi level.[29] GO thin films with lateral resistivity values in excess of 10^5 ohm/cm as the hole blocking layer in P3HT:PC_{61}BM PSCs. It must be clarified that the vertical resistivity of GO is an order of magnitude lower (~10^3–10^4 ohm/cm) than lateral resistivity. This is attributed to the fact that the sp^2 clusters are isolated laterally but are in contact with the electrodes in a sandwich structure. Thus, carriers (both holes and electrons) can be injected and transported via the isolated sp^2 clusters. Chhowalla et al.[20] have reported enhanced device performance of PSCs when GO was used as HTL. The efficiency of PSCs with a GO layer was comparable to the devices fabricated with PEDOT:PSS. The enhancement of device performance is mainly due to a the large band gap of GO (~3.6 eV) which blocks electron flow towards the anode and thus effectively suppresses the charge carrier recombination.[20,30] Furthermore, GO plays a role as a doping agent for semi-conducting polymers to increase the electrical conductivity.[31] Hence, it has been reported that blending of GO and PEDOT:PSS improves hole injection in PSCs.[32–34]

In previous reports,[19,35] a water-soluble and self-doped conducting copolymer based on polyaniline, poly(styrenesulfonic acid)-graft-polyaniline (PSSA–*g*–PANI), was synthesized and utilized as the hole transport material for P3HT:PC_{61}BM-based BHJ solar cells. Due to unique high optical transparency in the UV–vis region and high conductivity of PSSA–*g*–PANI, the device with PSSA–*g*–PANI as HTL exhibits higher PCE than the device with PEDOT:PSS. PSSA–*g*–PANI can be doped by GO because GO has

carboxylic acid group at edge site. Hence, taking advantages of both GO and PSSA–*g*–PANI may provide further enhancement of photovoltaic performance of PSCs.

In this work, PSSA–*g*–PANI/GO composites was prepared by adding GO into PSSA–*g*–PANI and used as HTL of PSCs for the purpose to further improve the PCE. A series of PSSA–*g*–PANI/GO composites with different GO concentrations was prepared in order to examine the effect of GO composition in the composite on the photovoltaic performance. The photovoltaic properties of the solar cell with the PSSA–*g*–PANI/GO composites as HTL were compared with the reference solar cell device with PEDOT:PSS as HTL.

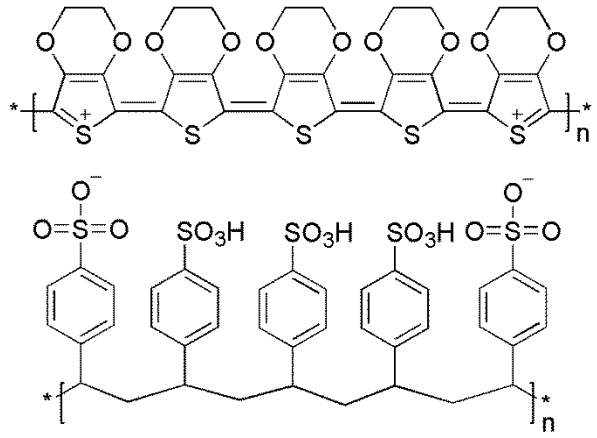

Figure 1.1 The chemical structure of conventional hole transport material, PEDOT:PSS.

Chapter 2. Experimental Section

2.1 Materials

Aniline (ACS reagent, ≥99.5%), Sodium 4-vinylbenzenesulfonate (technical, ≥90%), 4-Vinylaniline (97%) and Graphite (flakes, particle size>100 mesh) were purchased from Sigma-Aldrich Chemical Co.. Regioregular P3HT (55 kDa) was purchased from Rieke Metal Inc. PC61BM (>99.5%) was obtained from Nano-C and used as received without further purification. PEDOT:PSS (Baytron P VP AI 4083) was purchased from HC Stark.

2.2. Synthesis of PSSA–*g*–PANI

2.2.1. Synthesis of tert-butyl 4-vinylphenylcarbamate (BOC-AMS)

Scheme 2.1 shows the whole synthesis route of PSSA–*g*–PANI. A solution of aminostyrene (1.19 g, 10 mmol) in 10 ml of deionized water (H_2O) was added di-tert-butyl dicarbonate (Boc_2O, 2.40 g, 11 mmol). After vigorously stirring at 35 ^oC for 4 h, the mixture was extracted with dichloromethane (DCM, 25 ml). The organic layer was dried by anhydrous sodium sulfate (Na_2SO_4) and filtered. The filtrate was concentrated, and the residue was purified by flash chromatography (FC) (ethyl acetate/hexane = 2/8) to give 2.18 g white solid (yield: 99%). ^1H NMR (300 MHz, $CDCl_3$)

δ: 7.34 (s, 4H), 6.67 (dd, 1H, J = 10.8 Hz, J = 17.6 Hz), 6.47 (br, 1H), 5.66 (d, 1H, J = 17.6 Hz), 5.17 (d, 1H, J = 11 Hz), 1.53 (s, 9H)

2.2.2. Synthesis of P(SSNa-co-BOC-AMS)

P(SSNa-co-BOC-AMS) was synthesized by copolymerizing sodium 4-vinylbenzenesulfonate (SSNa) and t-BOC-AMS by using azobisisobutyronitrile (AIBN) as an initiator. SSNa (2.82g, 13 mmol), t-BOC-AMS (0.15g, 0.65 mmol), and AIBN (53mg) were dissolved in 50 ml of dimethyl sulfoxide (DMSO) and polymerized at 80 ^{o}C for 15 h under N^2 atmosphere. After polymerization, the product was precipitated with acetone, filtered, washed several times with acetone, and dried in a vacuum oven at 50 ^{o}C for 24 h. ^{1}H NMR spectra (300 MHz, DMSO-*d*6) of P(SSNa-co-BOC-AMS) shows the peak at 1.5 ppm (–CH3).

2.2.3. Synthesis of PSSA–*g*–PANI

Elimination of the BOC group from P(SSNa-co-BOC-AMS) and ion exchange of Na^+ with H^+ were carried out under acidic conditions. P(SSNa-co-BOC-AMS) (1.0 g) was added to 30 ml of HCl aqueous solution (1 M) at 30 ^{o}C for 1 h under stirring to yield P(SSA-co-AMS), and then the solution temperature was lowered to 0 ^{o}C. For graft copolymerization of aniline (ANI) onto P(SSA-BOC-AMS), ANI (0.086 g) was added to the above copolymer solution for 0.5 h with stirring, and then 20 ml of ammonium persulfate (0.25 g)/HCl aqueous solution (1 M) was dropwise added at 0 ^{o}C. After 6 h of reaction, a dark green solution was obtained and then filtered.

The filtered solution was further purified by dialysis using a semipermeable membrane (molecular weight cutoff, 3500). ^{1}H NMR spectra (300 MHz, DMSO-*d*6) of PSSA–*g*–PANI shows multiple peaks at 7.0, 7.1, 7.2 and 7.3 ppm, which are assigned to hydrogens in phenyl and quinoid rings of PANI. The peak at 1.5 ppm, which is related to $–CH_3$, disappeared because of removing BOC group in 1 M HCl solution.

2.3. Synthesis of graphene oxide

All reagents were purchased from Sigma Aldrich and were used without further purification. Graphite flake was oxidized by a modified Hummers method. In the pretreatment step that ensures complete oxidation, potassium persulfate (10 g) and phosphorus pentoxide (10 g) were added in sulfuric acid (50 ml) at 80 ^{o}C and stirred until the mixture was dissolved to prepare the oxidation solution. After graphite flake (10 g) was added to the oxidation solution and stirred at 80 ^{o}C for 4 h, the solution was diluted with 2 L of deionized (DI) water, stirred overnight, and filtered using ester cellulose membrane (Millipore, 0.2 μm pore size). The filtered mixture was washed with water to remove the oxidizing agents and dried in a vacuum oven.

Pretreated graphite (4 g), phosphorus pentoxide (62 g) and potassium manganite (24 g) were added to a solution of sulfuric acid (480 ml) and DI water (80 ml), and then the mixed solution was stirred slowly for 12 h. After the solution was sonicated in a bath-type sonicator (Hwashin Instrument, Power Sonic 410) for 1h, 35 wt% hydrogen peroxide (8 ml) and DI water (600 ml) were added to the solution.

Thereafter, the mixed solution was stirred vigorously at room temperature and sonicated for 2 h once a day during a week. To dissolve non-reacted potassium manganate solid, 30% hydrogen chloride (300 ml) and ethanol (300 ml) were added to the reaction mixture. Then the mixed solution was put into a metal sieve to sift out graphite. The filtered mixture was centrifuged at 7500 rpm for 1 h and the supernatant was decanted away for several times until pH of the supernatant was neutralized. The sediments were dried under vacuum overnight at room temperature.

For Hummer's method, concentrated H_2SO_4 (69 ml) was added to a mixture of graphite flakes (3.0 g, 1 wt equiv) and $NaNO_3$ (1.5 g, 0.5 wt equiv), and the mixture was cooled to 0 ^oC. $KMnO_4$ (9.0 g, 3 wt equiv) was added slowly in portions to keep the reaction temperature below 20 ^oC. The reaction was warmed to 35 ^oC and stirred for 30 min, at which time water (138 ml) was added slowly, producing a large exotherm to 98 ^oC. External heating was introduced to maintain the reaction temperature at 98 ^oC for 15 min, then the heat was removed and the reaction was cooled using a water bath for 10 min. Additional water (420 ml) and 30% H_2O_2 (3 ml) were added, producing another exotherm. After air cooling, the mixture was purified as described for the IGO above (sifting, filtration, multiple washings, centrifugations and decanting, vacuum drying) to give 1.2 g of brown solid.

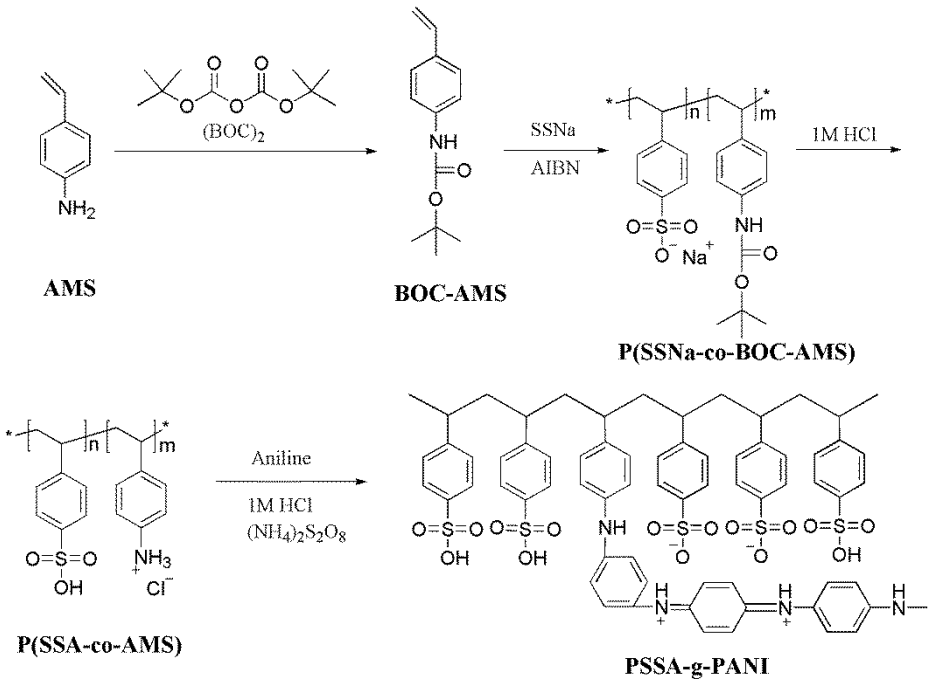

Scheme 2.1 The synthetic scheme of PSSA-*g*-PANI.

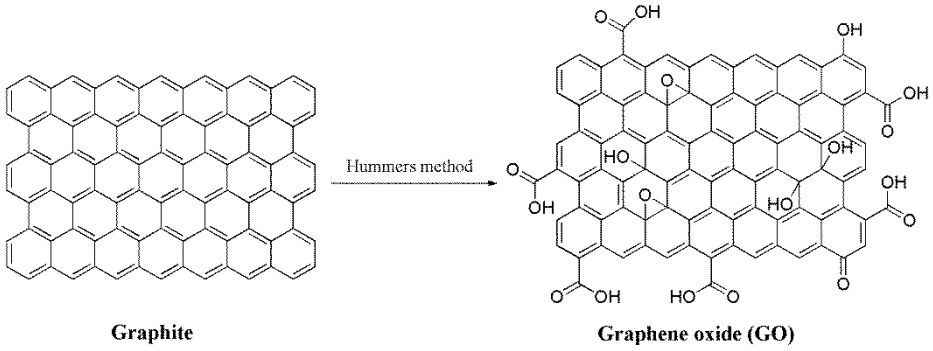

Scheme 2.2 The synthesis of graphene oxide (GO).

2.4. Preparation of PSSA–*g*–PANI/GO composites

GO was dispersed in deionized water (DI water) via bath-type sonication for 1hr and centrifuged at 4000 rpm for 10 min to remove aggregated GOs. The GO solution was added into PSSA–*g*–PANI aqueous solution and stirred for 24 hrs. 40 mg of PSSA–*g*–PANI was added into 2 ml DI water to prepare 2 wt% of solution. Various PSSA–*g*–PANI/GO composites were prepared by adding different amounts of GO (1.5, 2.5, 5.0, 7.5, 10.0 wt% with respect to PSSA–*g*–PANI) into 2 wt% PSSA–*g*–PANI aqueous solution.

2.5. Characterization

The chemical structures were identified by ^{1}H NMR (Avance DPX-300). Elemental analyses were recorded with a Jeol JMS600w in fast atom bombardment mode. The functional groups of GO was identified by FT-IR (Thermo Scientific, Nicolet 6700). The film thicknesses were determined by using atomic force microscopy. The transmittance of HTLs coated onto the bare glass were measured by using UV-Visible spectrophotometer (HP 8452A). The electrical conductivity was determined by a four-point sheet resistance measurement system (Napson, CRESBOX). The CV measurements were carried out by a three-electrode setup with platinum wires as both working electrode and counter electrode, and Ag/Ag^{+} was used as the reference electrode calibrated with ferrocene/ferrocenyl couple (Fc/Fc^{+}). A 0.1 M solution of tetrabutylammonium hexafluorophosphate (Bu_4NPF_6) in anhydrous acetonitrile was used as a supporting electrolyte. The hole transport layer material was coated onto the Pt working electrode

before the measurement. The XPS spectra of hole transport materials were obtained using an AXIS-HSi spectrometer (KRATOS).

2.6. Device fabrication and Characterization

For fabrication of solar cells with the standard device structure of glass/ITO/HTL/P3HT:$PC_{61}BM$/Al, ITO-coated glass (15 ohm/sq) was first cleaned with acetone and isopropyl alcohol and then dried at 120 ^{o}C for 2 h. After spin-coating of HTL material on the ITO-coated glass, the device was dried at 120 ^{o}C for 30 min. A blend solution of P3HT and PCBM was then spin-coated at 800 rpm for 40s, where the blend solution was prepared by dissolving 24 mg of blend (the weight ratio of P3HT:$PC_{61}BM$=1:0.8) in 1 mL of 1,2-dichlorobenzene. Al (100 nm thickness) was thermally evaporated under vacuum lower than 10^{-6} Torr on the top of the active layer. The device was thermally annealed at 150 ^{o}C for 10 min under nitrogen atmosphere. The photovoltaic performance was measured under nitrogen atmosphere inside the glove box.

The current density–voltage (*J*–*V*) characteristics were measured with a Keithley 4200 source-meter under AM 1.5 G (100 mW/cm^2) simulated by a Newport Oriel solar simulator. The light intensity was calibrated using a NREL certified photodiode and light source meter prior to each measurement. The active area was determined at 4 mm^2 by attaching a shadow mask onto solar cell device.

The hole-only device was fabricated with the same device configuration as the solar cell device except the anode material (Au was used instead of Al).

Au (40 nm thickness) was thermally evaporated under vacuum lower than 10^{-6} Torr on the top of the active layer. The hole mobility of the device was measured under the identical condition to the condition for optimized photovoltaic cells and calculated from the space-charge limited *J*–*V* curve using the Mott-Gurney law.

The external quantum efficiency (EQE) values were measured using a lock-in amplifier with a current preamplifier under short circuit current state with illumination of monochromatic light (K3100, McScience Co.). The light intensity at each wavelength was calibrated with a standard single-crystal Si cell. The solar cell devices for EQE measurement were fabricated with the same device configuration as the solar cell device.

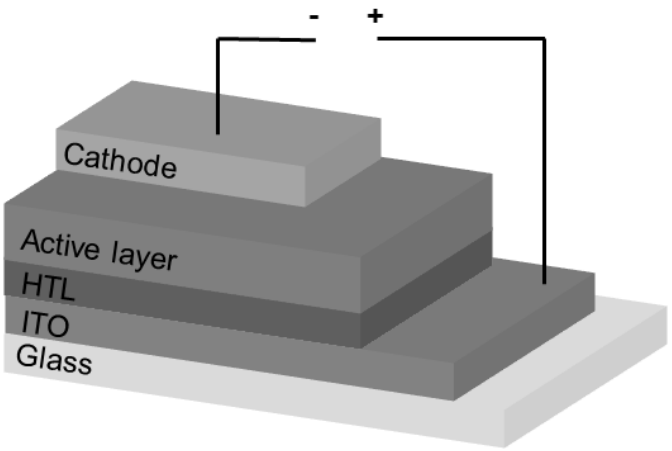

Figure 2.1 The device structure of polymer solar cell used in this research.

Chapter 3. Results and Discussion

3.1. Synthesis and Characterization

The chemical structures of PSSA–*g*–PANI, GO, and PSSA–*g*–PANI/GO composite are represented in Figure 3.1. The chemical structures of tert-Butyl 4-vinylphenylcarbamate is identified by ^{1}H NMR as shown in Figure 3.2. The molar ratio of AMS to SSA is 0.05 for P(SSNa-co-BOC-AMS). The molar ratio of ANI to SSA is 0.2 for PSSA–*g*–PANI. The molar ratio for the polymers is identified by elemental analysis.

The functional group of GO is identified by FT-IR as shown in Figure 3.3. Various oxygen configurations in the structure of GO include the vibration modes of epoxide (C–O–C) (1230–1320 cm^{-1}, asymmetric stretching; ~850 cm^{-1}, bending motion), sp^2-hybridized C=C (1500-1600 cm^{-1}, in-plane vibrations), Carboxyl (COOH) (1650–1750 cm^{-1} including C–OH vibrations at 3530 cm^{-1} and 1080 cm^{-1}), ketonic species (C=O) (1600–1650 cm^{-1}, 1750 cm^{-1}) and hydroxyl (namely phenol, C–OH) (3200–3500 cm^{-1} and 1070 cm^{-1}) with all C–OH vibrations from COOH and H_2O. Composites of PSSA–*g*–PANI/GO are simply prepared by adding GO into PSSA–*g*–PANI aqueous solution, because both GO and PSSA–*g*–PANI are soluble in water. Prepared PSSA–*g*–PANI/GO composite solution is composed of 40 mg of PSSA–*g*–PANI and 1.5, 2.5, 5.0, 7.5, 10.0 weight ratio with respect to weight of PSSA–*g*–PANI in 2 ml DI water. Morphology of the composites is studied by atomic force microscopy as shown in Figure 3.4. Average size of

GO sheets is 1–2 μm, and thickness is around 1 nm, which means the layer number of GO is monolayer. This well dispersed GO results in hydrophilic nature of GO.

3.2. Optical properties

To achieve high performance of PSCs, the active layer should harvest a large amount of light, and therefore a highly transparent HTL material should be used in PSCs since the light is passed through the HTL prior to the active layer. In a previous report,[19] the light absorption of P3HT:PC_{61}BM through PSSA–*g*–PANI was enhanced compared to the absorption of P3HT:PC_{61}BM through PEDOT:PSS in the 450–650 nm range because of the higher transparency of PSSA–*g*–PANI.

The transmittances of PEDOT:PSS, PSSA–*g*–PANI, PSSA–*g*–PANI/GO with different GO concentrations are shown in Figure 3.5 and Table 3.1. PANI, PANI/GO(1.5), PANI/GO(2.5), PANI/GO(5.0), PANI/GO(7.5) and PANI/GO(10.0) mean PSSA–*g*–PANI, PSSA–*g*–PANI with GO 1.5, 2.5, 5.0, 7.5, 10.0 wt%. The transmittance of HTL materials is 95.9, 97.1, 97.0, 96.8, 96.3, 95.6 and 95.3 % at 550 nm for PEDOT:PSS, PANI, PANI/GO(1.5), PANI/GO(2.5), PANI/GO(5.0), PANI/GO(7.5) and PANI/GO(10.0), respectively. The reason why the transmittance was measure at 550 nm is that the main absorption wavelength of P3HT is around 550 nm.

The transmittance of PSSA–*g*–PANI/GO films slightly decreases as the amount of GO in the composites increases. The PSSA–*g*–PANI, PSSA–*g*–PANI with GO 2.5 wt%, and PSSA-g-PANI with GO 5.0 wt% afford better

optical transmittance (> 96%) than PEDOT:PSS in the range from 450 to 600 nm of wavelength. Therefore it is expected that the devices of PSSA–*g*–PANI, PSSA–*g*–PANI with GO 2.5, 5.0 wt% would make the active layer harvest more light than PEDOT:PSS in PSCs based on P3HT:$PC_{61}BM$ blend because 450–600 nm is the major absorption range of P3HT.

3.3 Electrical properties

For improving charge selectivity at the electrodes and minimize the energy barrier for charge extraction, HTL with electron-blocking properties is inserted between the anode and BHJ active layer. The doped conductive polymer, PEDOT:PSS, is commonly used as HTL material because of its solution precessability, work function and sufficient electrical conductivity. However, PEDOT:PSS has a low electrical conductivity (0.008 S/cm). It often limits the hole transport from the active layer to anode in PSCs.

The important parameter of HTL for high performance PSCs is electrical conductivity. It has been reported that the enhanced performance of PSCs was achieved by using highly conductive PEDOT:PSS which is doped with various polyalcohols[33], or prepared from solvent mixture.[34] The electrical conductivity of HTL materials were measured by four-point sheet resistances and is shown in Figure 3.6 and Table. 3.1. We have already demonstrated that the electrical conductivity of PSSA–*g*–PANI was much higher than that of PEDOT:PSS and the resulting performance of PSCs based on PSSA–*g*–PANI was much improved than that with PEDOT:PSS.[19] The electrical conductivity of PSSA–*g*–PANI was controlled by changing the molar ratio

of ANI to SSA during polymerization. The optical and electrochemical characteristics of all the PSSA–*g*–PANIs were almost same. When the molar ratio of ANI/SSA for PSSA–*g*–PANI is 0.2, PSSA–*g*–PANI showed the highest electrical conductivity (0.850 S/cm). The copolymers with a low ratio of ANI to SSA exhibited very low conductivity because of a small amount of conductive polyaniline part. However, the electrical conductivity starts to decrease as the ratio of ANI to SSA. This can be explained by considering the doping effect of PSSA to PANI.

To further improve the electrical conductivity of PSSA–*g*–PANI films, GO was introduced to the PSSA–*g*–PANI film because the electrical conductivity of PEDOT:PSS was improved by GO doping in previous report.[31] Because the PSSA–*g*–PANI shows high electrical conductivity as the PANI is doped by sulfonic acid groups of PSSA, PANI might be further doped by the carboxylic acid groups of GO in the same mechanism.

As a result, the PSSA–*g*–PANI/GO composites showed higher conductivity as compared to PSSA–*g*–PANI (0.725 S/cm) and PEDOT:PSS (0.008 S/cm). Especially, PSSA–*g*–PANI with GO 1.5, 2.5, 5.0 wt% showed a high conductivity around 1 S/cm at around 40 nm thickness of the films. However, as the GO was introduced more than 5.0 wt%, the electrical conductivity decreases with increase of GO concentration in the composite of GO in PSSA–*g*–PANI/GO. This electrical conductivity decrease of the composites is attributed to the strong insulating property of GO, which prohibits efficient charge transport in the composite film.

3.4 Photoelectrical properties

Polyaniline (PANI) exists in a variety of forms that differ in chemical and physical properties. The most common protonated emeraldine has a conductivity at the semiconductor level of the order of 100 S/cm, which is many orders of magnitude higher than that of common polymers ($<10^{-9}$ S/cm). It has been demonstrated that the base form of PANI can be converted to its salt form by proton doping, in which the electron number on the polymer chain does not change after protonation. It seems that proton doping can take place on the amine and the imine segment of the polyemeraldine chain. As compared to non-protonated emeraldine PANI, the protonated PANI has much higher electrical conductivity.35 It imply that protonation of PANI is important to enhance the electrical conductivity of PANI.

To further improve the electrical conductivity of PSSA–*g*–PANI, GO was added in PSSA–*g*–PANI, where PANI part can be doped with the carboxylic acid groups in GO (Figure 3.1). For identifying the doping of PANI with carboxylic acid, the N 1s X-ray photoelectron spectroscopy (XPS) spectra of PANI and PANI/GO(10.0) are measured and compared, as shown in Fig. 3.7 and Table 2. When the N 1s spectra are deconvoluted into two peaks corresponding to benzenoid diamine nitrogen and protonated nitrogen centered at 399.6 eV and 401.5 eV, respectively,[36,37] it reveals that the relative fraction of protonated nitrogen atoms (60.5%) in PANI/GO(10.0) is larger than that of PANI (51.9%), indicating that PANI is doped with carboxylic acid groups of GO. Full

width at half maximum (FWHM) values for proton doped N^+ peak are 2.210 and 2.091 for PANI and PANI/GO(10.0). As a result, the electrical conductivities of PSSA–*g*–PANI/GO composites (>0.833 S/cm) are higher than that of PSSA–*g*–PANI (0.725 S/cm). It is also observed that the electrical conductivity increases with increasing the GO loading in the composites up to 5.0 wt%. However, the electrical conductivity starts to decrease when the GO concentration is further increased above 5.0 wt%. The decrease in electrical conductivity with increasing the GO content is attributed to the insulating property of GO.

3.5 Electrochemical properties

To improve the photovoltaic performance of polymer solar cells, the buffer layer between the anode and the active layer is frequently used. The architecture of the organic photovoltaic structure is important, so matching the energy level of the active layer with the work function of electrodes becomes necessary. HTL materials should be wide bandgap p-type materials, and also the energy level of HTLs must be located between the Fermi level of ITO and the highest occupied molecular orbital (HOMO) level of active layer donor material. In order to investigate the role of the composites as HTL, HOMO level of the composites was measured by the cyclic voltammetry (CV). The electrochemical data of the HTL materials is obtained from the oxidation CV curve. The HOMO energy level of the HTL materials was calculated using the equation: HOMO = –[E_{OX} – $E_{1/2}$(ferrocene) + 4.8] V, where E_{OX} is the onset oxidation potential of the

materials and $E_{1/2}$(ferrocene) is the onset oxidation potential of ferrocene vs. Ag/Ag^{+}. The HOMO energy level of PEDOT:PSS, PSSA–*g*–PANI, and PSSA–*g*–PANI/GO composites are shown in Figure 3.8 and Table 3.1. The HOMO energy levels of PEDOT:PSS, PANI, PANI/GO(1.5), PANI/GO(2.5), PANI/GO(5.0), PANI/GO(7.5), PANI/GO(10.0) are –4.81, –4.89, –4.89, –4.89, –4.85, –4.87 and –4.83, respectively. The HOMO energy level of HTL materials was calculated by measuring onset of oxidation peak. The energy levels of the polymers and composites (ca. 4.8 eV) are a good match to both the work function of ITO (4.7–4.8 eV in air) and the HOMO level of P3HT (5.0–5.1 eV) for efficient hole transport from P3HT to ITO. This well matched energy level suggests that the composites is an excellent candidate to the conventional PEDOT:PSS for HTL of PSCs.

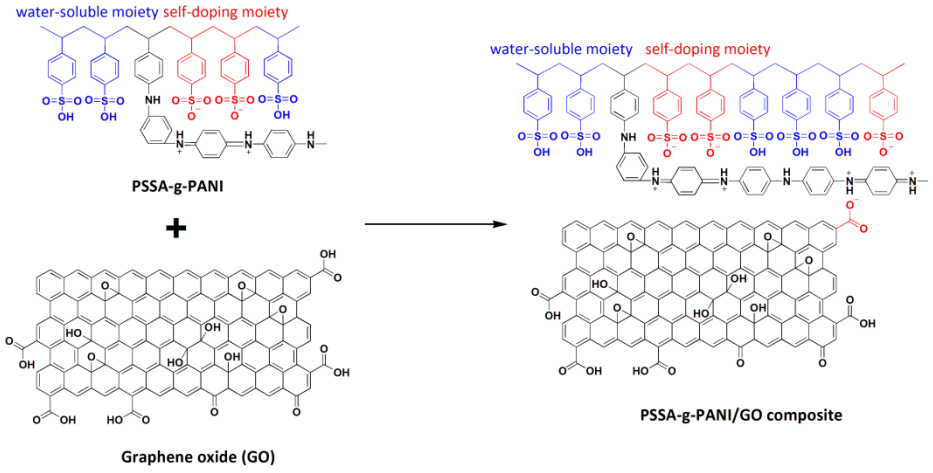

Figure 3.1 Chemical structures of PSSA–*g*–PANI, GO and PSSA–*g*–PANI/GO composite.

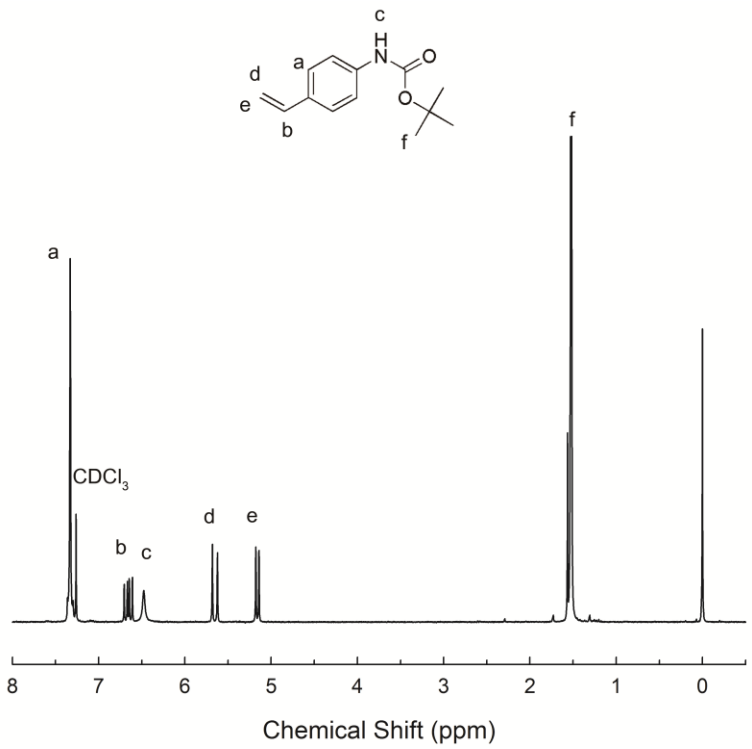

Figure 3.2 Chemical structure and ^{1}H NMR spectrum of tert-Butyl 4-vinylphenylcarbamate.

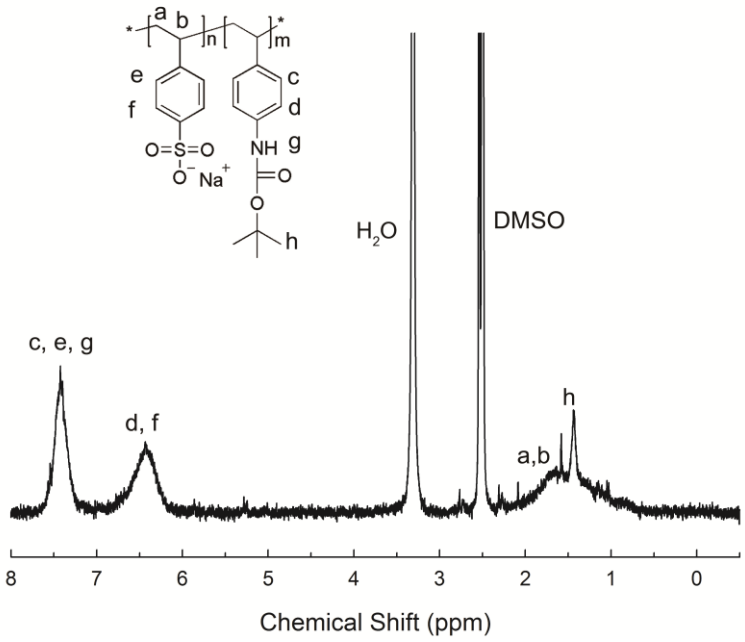

Figure 3.3 Chemical structure and ^{1}H NMR spectrum of P(SSNa-co-BOC-AMS).

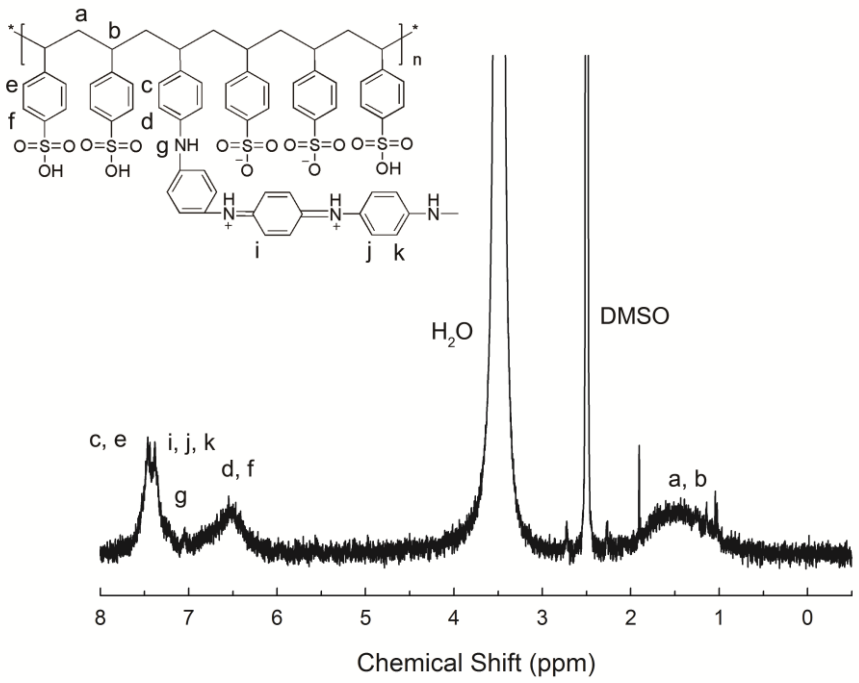

Figure 3.4 Chemical structure and ^{1}H NMR spectrum of PSSA–*g*–PANI.

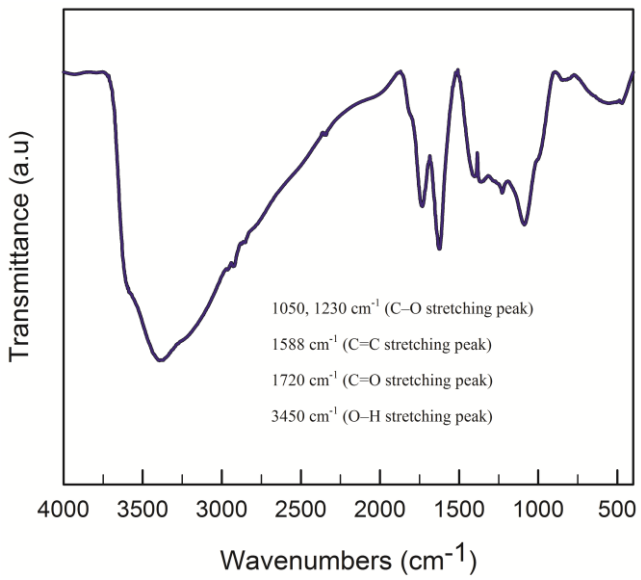

Figure 3.5 FT-IR spectrum of GO.

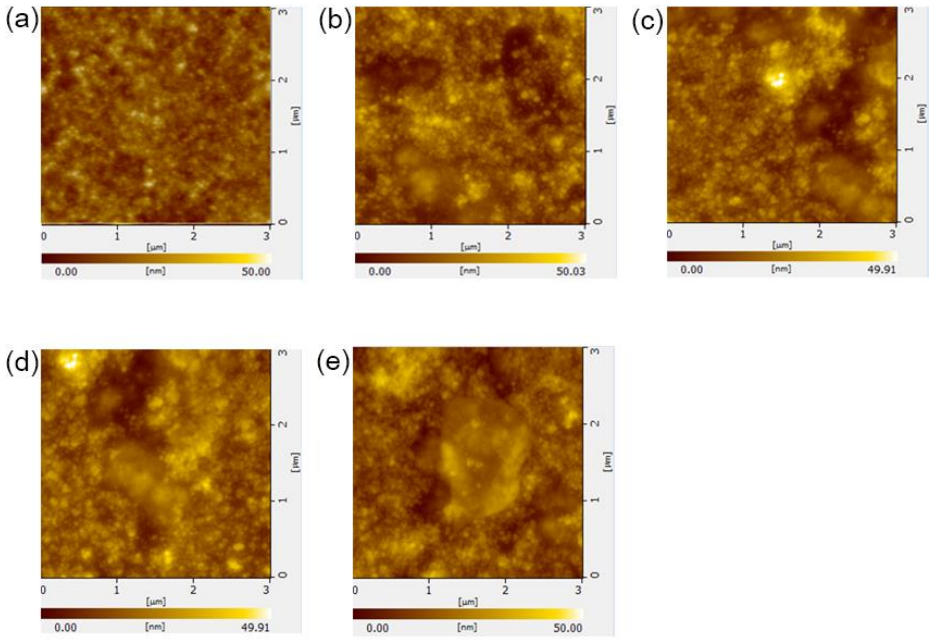

Figure 3.6 AFM images of PSSA–*g*–PANI and PSSA–*g*–PANI/GO composites. (a) PSSA–*g*–PANI (b) PSSA–*g*–PANI/GO(2.5) (c) PSSA–*g*–PANI/GO(5.0) (d) PSSA–*g*–PANI/GO(7.5) (e) PSSA–*g*–PANI/GO(10.0).

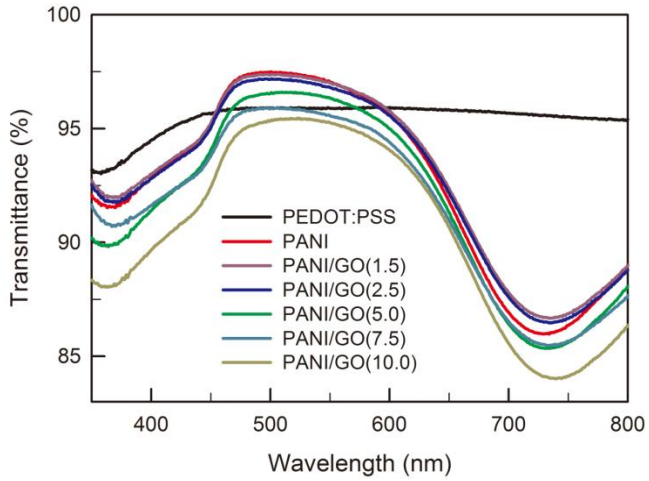

Figure 3.7 Transmittances of PEDOT:PSS, PSSA–*g*–PANI and PSSA–*g*–PANI/GO composite films, where the film thickness is shown in Table 1.

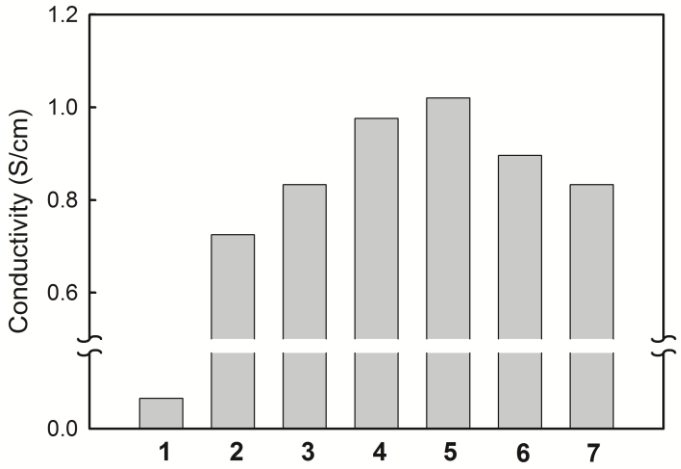

Figure 3.8 The electrical conductivities of PEDOT:PSS, PSSA–*g*–PANI and PSSA–*g*–PANI/GO composite films. 1, 2, 3, 4, 5, 6 and 7 mean PEDOT:PSS, PSSA–*g*–PANI and PSSA–*g*–PANI/GO (1.5, 2.5, 5.0, 7.5, 10.0), respectively.

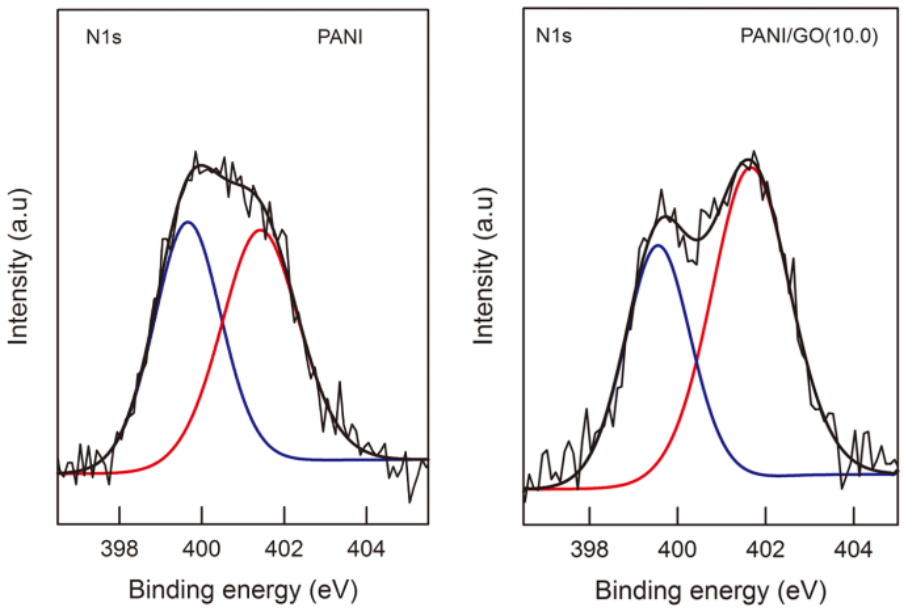

Figure 3.9 N 1s XPS spectra of PANI and PANI/GO(10.0), where the two peaks correspond to bezenoid diamine nitrogen (blue line) and protonated nitrogen (red line) centered at 399.6 eV and 401.5 eV, respectively.

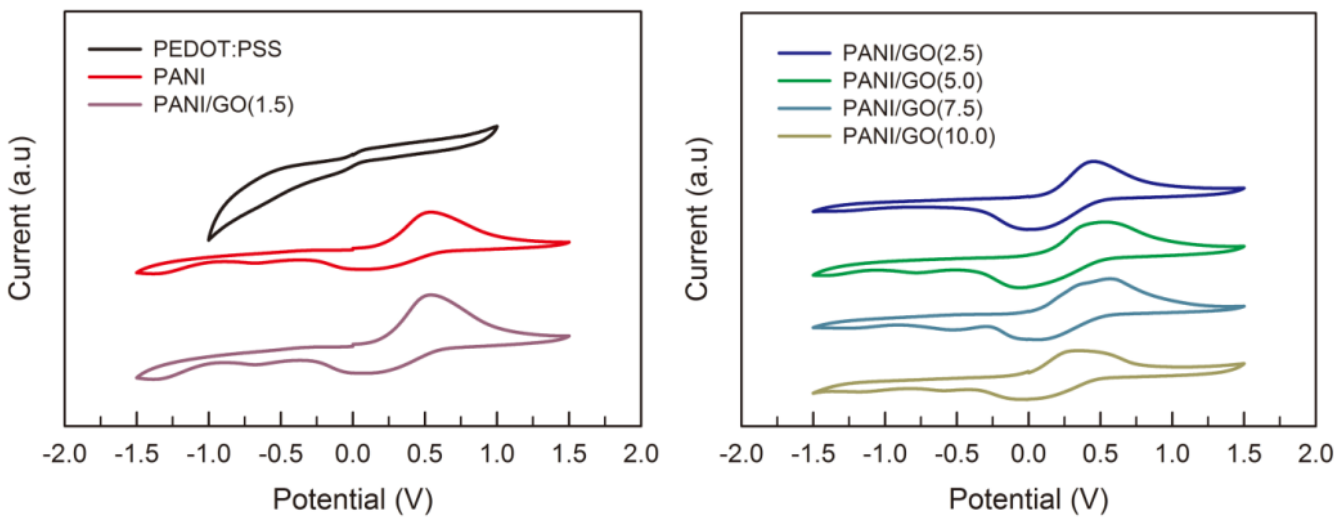

Figure 3.10 Cyclic voltammetry curves of PEDOT:PSS, PSSA–*g*–PANI and PSSA–*g*–PANI/GO composites.

Table 3.1 Film thickness, optical transmittance, electrical conductivity and HOMO energy level of the composite films.

HTL material	GO wt%	Film thickness (nm)	Transmittance (%)[a]	Conductivity (S/cm)	HOMO (eV)
PEDOT:PSS	–	37	95.9	0.008	– 4.81
PANI	0.0	41	97.1	0.725	– 4.89
PANI/GO(1.5)	1.5	43	97.0	0.833	– 4.89
PANI/GO(2.5)	2.5	40	96.8	0.976	– 4.89
PANI/GO(5.0)	5.0	39	96.3	1.020	– 4.85
PANI/GO(7.5)	7.5	42	95.6	0.896	– 4.87
PANI/GO(10.0)	10.0	40	95.3	0.833	– 4.83

[a]The transmittance is measured at 550 nm.

Table 3.2 Contribution of nitrogen groups resulting from the fitting of Gaussian components to the N(1s) photoelectron spectra.

Materials		Binding energy (eV)	FWHM	Relative percentage (%)
PANI	–NH–	399.6	1.931	48.1
	N^+	401.6	2.210	51.9
PANI/GO(10.0)	–NH–	399.6	1.768	39.5
	N^+	401.4	2.091	60.5

3.6 Photovoltaic properties

The *J*–*V* curves of PSCs with PSSA–*g*–PANI/GO composites as HTL are shown in Figure 3.11. The polymer solar cells were fabricated with the conventional device configuration of glass/ITO/HTL/P3HT:$PC_{61}BM$/Al. The short-circuit current density (J_{SC}), open-circuit voltage (V_{OC}), fill factor (FF) and PCE values are summarized in Table 3.3. All polymer solar cell devices were annealed at 150 ^{o}C for 10 min after Al vacuum-deposited. In the device with P3HT:$PC_{61}BM$, thermal annealing method is important to enhance the performance of the device. This performance enhancement results from two effects: higher nanoscale crystallinity and improved microstructure with demixing between the two components in the bulk heterojunction films after thermal annealing. Since the V_{OC} of PSCs in linearly dependent on the difference between the HOMO energy level of the electron donor and the LUMO energy level of the electron acceptor, the V_{OC}s may not be affected with different hole transporting materials in this research. Therefore, there is no significant difference of V_{OC} in the devices with different HTL materials.

The solar cell devices with PANI or PANI/GOs exhibit higher J_{SC} and higher PCE than the device with PEDOT:PSS. Especially, the device with PANI/GO(2.5) shows the highest PCE (4.23%), which is 23% and 10% higher than the devices with PEDOT:PSS and PSSA–*g*–PANI, respectively. The J_{SC}s of the device prepared with PEDOT:PSS, PSSA–*g*–PANI, PANI/GO(1.5), PANI/GO(2.5), PANI/GO(5.0), PANI/GO(7.5) and PANI/GO(10.0) are 9.76, 10.07, 10.25, 10.66, 9.82, 9.32 and 9.69 mA/cm^2

respectively. This higher J_{SC} is attributed to higher optical transmittance and higher electrical conductivity of PSSA–*g*–PANI/GO composites as compared to those of PEDOT:PSS or PSSA–*g*–PANI. The higher transparency of HTL results in larger light absorption of P3HT and higher J_{SC}. This is manifested by the fact that the more transparent characteristic of PSSA–*g*–PANI and PSSA–*g*–PANI/GO composites exhibits a high value of incident photon-to-current efficiency in the wavelength range from 450 to 600 nm, which corresponds to the main absorption of P3HT. When the J_{SC}s calculated from the external quantum efficiency (EQE) spectra (Figure 3.12) are compared, it also reveals that the devices with PSSA–*g*–PANI/GO(1.5) and PSSA–*g*–PANI/GO(2.5) composites exhibit higher J_{SC} than the devices with PEDOT:PSS and PSSA–*g*–PANI.

It has been reported that the hole mobility increase for the device allows more balance charge transport in the active layer, thus improving J_{SC} of the device in other reports.[38–40] To verify the vertical charge transport of the PSC devices, the hole mobility were measured by the space charge limited current method. The hole mobility is estimated from the $J^{1/2}$–V characteristics at low voltage region (Figure 3.13 and Table 3.4) using the Mott-Gurney square law,[41,42]

$$J = (9/8)\varepsilon_r\varepsilon_0\mu_h(V^2/L^3),$$

where ε_r is the dielectric permittivity of the active layer, ε_0 is the vacuum permittivity, L is the thickness of the active layer, and μ_h is the hole mobility.

It should be noted here that the hole mobility was measured using the same device structure as the solar cell device except for the cathode material (Au instead of Al), and that the obtained the hole mobilities are not for the active layer but for the complete device including the active layer and the hole transport layers. The hole mobilities of the device prepared with PEDOT:PSS, PSSA–*g*–PANI, PANI/GO(1.5), PANI/GO(2.5), PANI/GO(5.0), PANI/GO(7.5) and PANI/GO(10.0) are 2.05×10^{-4}, 6.33×10^{-4}, 4.20×10^{-4}, 7.90×10^{-4}, 5.71×10^{-4}, 6.18×10^{-4} and 3.34×10^{-4} $cm^2V^{-1}s^{-1}$, respectively. The device prepared with PANI/GO(2.5) shows the highest hole mobility (7.90×10^{-4} $cm^2V^{-1}s^{-1}$), which may contribute to the largest J_{SC} of the device with PANI/GO(2.5) composite as HTL.

FF characterizes how square the *J*–*V* curve is and it represents how easy the photogenerated carriers can be extracted out of a photovoltaic device. The ideal value of FF is unity (100 %), when the *J*–*V* curve is rectangle shape. The series resistance (R_s) and shunt resistance (R_{sh}) in PSCs are useful parameters to evaluate the contact properties of the BHJ/electrode interface. R_s induces a voltage drop on itself, so it can divide the applied voltage from the diode. It determines where the current mainly flows. R_{sh} has the effect of dividing current from diode, which makes it exhibit the opposite trend to that of R_s. It denotes the current losses in the cells, current leakage from the pinholes in the film or the current leakage by the traps. Contact resistance and charge recombination at the interface are directly related to R_s and R_{sh}, respectively: high R_s results in large contact resistance and low R_{sh} reflects large charge recombination. When PANI/GO(2.5) is used as HTL instead of

PEDOT:PSS, the R_s decreases from 4.31 Ω cm^2 to 2.49 Ω cm^2 and the R_{sh} increases from 1.61 kΩ cm^2 to 2.71 kΩ cm^2, indicating that PANI/GO(2.5) has better ohmic contact at the interface than PEDOT:PSS and that the charge recombination at the BHJ/anode interface is effectively suppressed. The FFs of the device prepared with PEDOT:PSS, PSSA–*g*–PANI, PANI/GO(1.5), PANI/GO(2.5), PANI/GO(5.0), PANI/GO(7.5) and PANI/GO(10.0) are 0.56, 0.60, 0.61, 0.62, 0.61, 0.61 and 0.62. The devices with PSSA–*g*–PANI/GO composite show higher FF than the device with PEDOT:PSS. It can be explained by that the device with PSSA–*g*–PANI/GO composite exhibits higher R_{sh} and lower R_s, as compared to the device with PEDOT:PSS.

As a result, the FF of PANI/GO(2.5) is higher than the device with PEDOT:PSS. It is concluded that PSSA–*g*–PANI/GO composites transport holes more efficiently and lowers the leakage current as compared to PEDOT:PSS. Due to these optical and electrochemical characteristics, the PSC with PSSA–*g*–PANI/GO composites as HTL exhibits a higher PCE value than that with PEDOT:PSS.

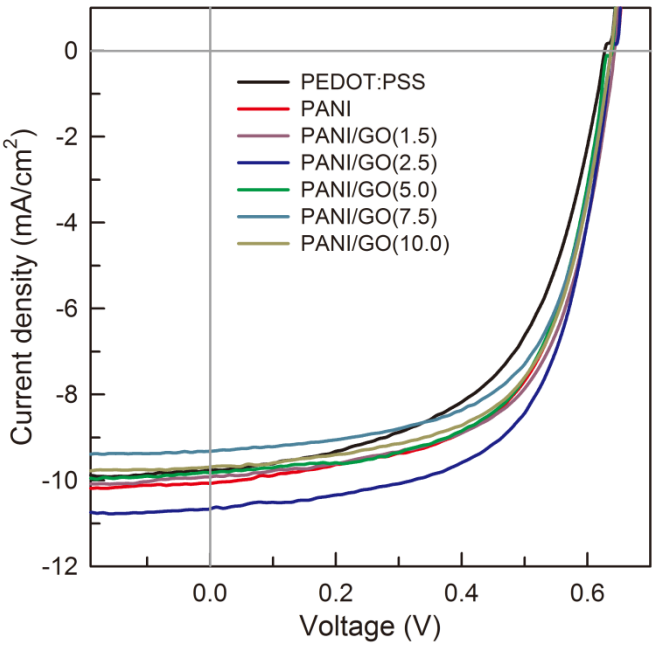

Figure 3.11 *J–V* curves measured under AM 1.5 G (100 mW/cm^2) of P3HT:$PC_{61}BM$ solar cell devices with PEDOT:PSS, PSSA–*g*–PANI, and PSSA–*g*–PANI/GO composites as HTL.

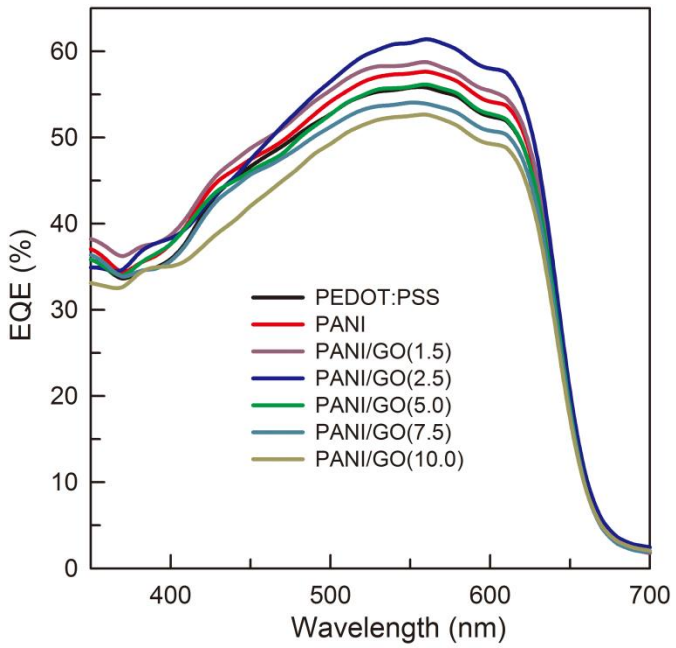

Figure 3.12 External quantum efficiency (EQE) spectra of polymer solar cell devices with PEDOT:PSS, PSSA–*g*–PANI, and PSSA–*g*–PANI/GO composites as HTL. All devices were annealed at 150 ^{o}C for 10 min.

Table 3.3 Photovoltaic parameters of the P3HT/$PC_{61}BM$ PSC devices with different hole transport layer materials. The shunt resistance (R_{sh}) and series resistance (R_s) are measured from the dark *J–V* curve.

HTL material	V_{OC} (V)	J_{SC} (mA/cm^2)	FF	PCE (%)[a]	R_{sh} (kΩ cm^2)	R_s (Ω cm^2)
PEDOT:PSS	0.63	9.76	0.56	3.44(3.41)	1.61	4.31
PANI	0.64	10.07	0.60	3.87(3.85)	2.10	3.35
PANI/GO(1.5)	0.64	10.25	0.61	4.00(3.95)	2.89	2.82
PANI/GO(2.5)	0.64	10.66	0.62	4.23(4.18)	2.72	2.49
PANI/GO(5.0)	0.64	9.82	0.61	3.83(3.83)	2.92	2.70
PANI/GO(7.5)	0.64	9.32	0.61	3.64(3.58)	1.87	2.64
PANI/GO(10.0)	0.64	9.69	0.62	3.84(3.71)	2.02	2.82

[a]The values in parenthesis denote average values of at least 4 devices.

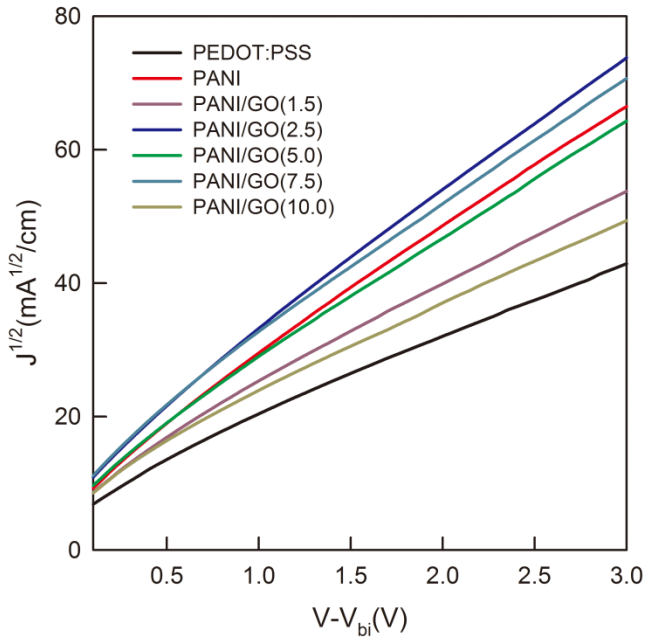

Figure 3.13 $J^{1/2}$–V characteristics of hole-only devices with PEDOT:PSS, PSSA–*g*–PANI and PSSA–*g*–PANI/GO composites as HTL.

Table 3.4 The hole mobilities of the hole-only devices with different hole transport layer materials. The hole-only device is composed of ITO/HTLs/P3HT:$PC_{61}BM$/Au.

HTL materials	μ_h ($cm^2V^{-1}s^{-1}$)
PEDOT:PSS	2.05×10^{-4}
PANI	6.33×10^{-4}
PANI/GO(1.5)	4.20×10^{-4}
PANI/GO(2.5)	7.90×10^{-4}
PANI/GO(5.0)	5.71×10^{-4}
PANI/GO(7.5)	6.18×10^{-4}
PANI/GO(10.0)	3.34×10^{-4}

3.7 Discussions

PSSA–*g*–PANI/GO composites with high optical transparency and high electrical conductivity, has been successfully prepared. The effects of optical transparency and electrical conductivity of this PSSA–*g*–PANI/GO composite on the performance of PSCs were studied in this research. The composites showed unique high transparency in the UV-Vis region (especially 450–600 nm) and high electrical conductivity (1.02 S/cm) of the composites with no significant HOMO energy level difference of the composites. The device of PSSA–*g*–PANI with GO 2.5 wt%, which has high transmittance and electrical conductivity, exhibited the highest PCE of 4.23%. The J_{SC} and *FF* both increased with no significant change of V_{OC}. V_{OC}s are not affected with the different hole transporting materials.

Increased J_{SC} and FF are verified by external quantum efficiency and hole mobility. The enhancement of hole mobility for the device allows more balance charge transport in the active layer, which can explain the enhanced J_{SC} and FF of the devices with PSSA–*g*–PANI/GO composites as HTL. Consequently, we have demonstrated a 23% enhancement in PCE by introducing GO into PSSA–*g*–PANI as HTL of PSCs, compared to the device with conventional hole transport material PEDOT:PSS.

Chapter 4. Conclusion

A new class of HTL materials, PSSA–*g*–PANI/GO composites with high optical transparency and high electrical conductivity, has been developed. When PSSA–*g*–PANI with 2.5 wt% GO loading was used as HTL in PSCs, the P3HT:$PC_{61}BM$-based solar cell device exhibited a PCE of 4.23%, which is 23% higher than the device with PEDOT:PSS (3.44%). The enhanced performance of PSCs is mainly caused by increase of J_{SC} and FF. The enhanced J_{SC} and FF can be explained by that PSSA–*g*–PANI/GO composite shows much higher electrical conductivity and hole mobility of the device, as compared to the device with PEDOT:PSS.

In short, PSSA–*g*–PANI/GO composite has strong potential for a promising HTL material in PSCs to enhance the photovoltaic performance of organic solar cells.

Bibliography

(1) Brabec, C. J.; Sariciftci, N. S.; Hummelen, J. C. *Adv*. *Funct*. *Mater*. **2011**, 11, 15

(2) Yu, G.; Heeger, A. J. *J*. *Appl*. *Phys*. **1995**, 78, 4510

(3) Lee, J. U.; Cirpan, A.; Emrick, T.; Russell, T. P.; Jo, W. H. *J*. *Mater*. *Chem*. **2009**, 19, 1483

(4) Li, G.; Shrotriya, V.; Huang, J.; Yao, Y.; Moriatry, T.; Emery, K; Yang, Y. *Nat*. *Mater*. **2005**, 4, 864

(5) Ma, W.; Yang, C.; Gong, X.; Lee, K.; Heeger, A. J. *Adv*. *Funct*. *Mater*. **2005**, 15, 1617

(6) Miller, S.; Fanchini, G.; Lin, Y. Y.; Li, C.; Chen, C. W.; Su, W. F.; Chhowalla, M. *J*. *Mater*. *Chem*. **2008,** 18, 306

(7) Chiu, M. Y.; Jeng, U. S.; Su, M. S.; Wei, K. H. *Macromolecules*. **2010**, 43, 428

(8) Chen, D.; Nakahara, D.; Wei, D.; Nerdlund, D.; Russell, T. P. *Nano Lett*. **2011**, 11, 561

(9) Park, S. H.; Roy, A.; Beaupre, S.; Cho, S.; Coates, N.; Moon, J. S.; Moses, D.; Leclerc, M.; Lee, K.; Heeger, A. J. *Nat*. *Photonics*, **2009**, 3,

297

(10) Liang, Y.; Xu, Z.; Xia, J.; Tsai, S. T.; Wu, Y.; Li, G.; Ray, C.; Yu, L. *Adv*. *Mater*. **2010**, 22, E135

(11) Li, G.; Chu, C. W.; Shotriya, V.; Huang, J.; Yang, Y. *Appl*. *Phys*. *Lett*. **2006**, 88, 253503

(12) Tan, Z.; Qian, D.; Zhang, W.; Li, L.; Ding, Y.; Xu, Q.; Wang, F.; Li, Y. *J*. *Mater*. *Chem*. A **2013**, 1, 657

(13) Carter, S. A.; Angelopoulos, M.; Karg, S.; Brock, B. J.; Scott, J. C. *Appl*. *Phys*. *Lett*. **1997**, 70, 2067

(14) Brown, T. M.; Kim J. S.; Friend, R. H.; Cacialli, F.; Daik, R.; Feast, W. *J*. *Appl*. *Phys*. *Lett*. **1999**, 75, 1979

(15) Steim, R.; Kogler, F. R.; Brabec, C. J. *J*. *Mater*. *Chem*. **2010**, 20, 2499

(16) Ma, H.; Yip, H. L.; Huang, F.; Jen, A. K. Y. *Adv*. *Funct*. *Mater*. **2010**, 20, 1371

(17) Pingree, L. S. C.; MacLeod, B. A.; Ginger, D. S. *J*. *Phys*. *Chem*. *C* **2008**, 112, 7922

(18) Norman, K.; Madsen, M. V.; Gevorgyan, S. A.; Krebs, F. C. *J*. *Am*. *Chem*. *Soc*. **2010**, 132, 16883

(19) Jung, J. W.; Lee, J. U.; Jo, W. H. *J*. *Phys*. *Chem*. *C*, **2010**, 114, 633

(20) Li, S. S.; Tu, K. H.; Lin, C. C.; Chen, C. W.; Chhowalla, M. *ACS*

Nano **2010**, 4, 3169

(21) Liu, J.; Xue, Y.; Dai, L.; *J. Phys. Chem. Lett.* **2012**, 3, 1928

(22) Gao, Y.; Yip, H. L.; Chen, K. S.; O'Malley, K. M.; Acton, O.; Sun, Y.; Ting, G.; Chen, H.; Jen, A. K. Y. *Adv. Mater.* **2011**, 23, 1903

(23) Yun, J. M.; Yeo, J. S.; Kim, J.; Jeong, H. G.; Kim, D. Y.; Noh, Y. J.; Kim, S. S.; Ku, B. C.; Na, S. I. *Adv. Mater.* **2011**, 23, 4923

(24) Liu, X.; Kim, H.; Guo, L. J. *Org. Electron.* **2013**, 14, 591

(25) Schniepp, H. C.; Li, J. L.; McAllister, M. J.; Sai, H.; Herrera-Alonso, M.; Adamson, D. H.; Prud'homme, R. K.; Car, R.; Saville, D. A.; Aksay, I. A. *J. Phys. Chem. B* **2006**, 110, 8535

(26) Lerf, A.; He, H. Y.; Forster, M.; Klinowski, J. *J. Phys. Chem. B* **1998**, 102, 4477

(27) He, H. Y.; Klinowski, J.; Forster, M.; Lerf, A. *Chem. Phys. Lett.* **1998**, 287, 53

(28) Mattevi, C.; Eda, G.; Agnoli, S.; Miller, S; Mkhoyan, K. A.; Celik, O.; Mastrogiovanni, D.; Granozzi, G.; Garfunkel, E.; Chhowalla, M. *Adv. Funct. Mater.* **2009**, 19, 2577

(29) Eda, G.; Mattevi, C.; Yamaguchi, H.; Kim, H.; Chhowalla, M. *J. Phys. Chem. C* **2009**, 113, 15768

(30) Gao, Y.; Yip, H. L.; Hau, S. K.; O'Malley, K. M.; Cho, N. C.; Chen,

H.; Jen, A. K. Y. *Appl. Phys. Lett*. **2010**, 97, 203306

(31) Zeng, J. J.; Lin, Y. J. *J. Appl. Phys*. **2013**, 113, 064502

(32) Yin, B.; Liu, Q.; Yang, L.; Wu, X.; Liu, Z.; Hua, Y.; Yin, S.; Chen, Y. *J. Nanosci. Nanotechnol*. **2010**, 10, 1934

(33) Chang, H.; Wang, G.; Yang, A.; Tao, X.; Liu, X.; Shen, Y.; Zheng, Z. *Adv. Funct. Mater*. **2010**, 20, 2893

(34) Zhong, Z.; Dai, Y.; Ma, D.; Wang, Z. Y. *J. Mater. Chem*. **2011**, 21, 6040

(30) Bae, W. J.; Kim, K. H.; Park, Y. H.; Jo, W. H. *Chem. Commun*. **2003**, 22, 2768

(31) Marcano, D. C.; Kosynkin, D. V.; Berlin, J. M.; Sinitskii, A.; Sun, Z.; Slesarev, A.; Alemany, L. B.; Lu, W.; Tour, J. M. *ACS Nano*. **2010**, 4, 4806

(32) Chen, G. L.; Shau, S. M.; Juang, T. Y.; Lee, R. H.; Chen, C. P.; Suen, S. Y.; Jeng, R. J. *Langmuir* **2011** 27, 14563

(33) Zhang, F. L.; Gadisa, A.; Inganas, O.; Svensson, M.; Andersson, M. R. *Appl. Phys. Lett*. **2004**, 84, 3906

(34) Xia, Y.; Ouyang, J. *J. Mater. Chem*. **2011**, 21, 4927

(35) Chianga, J. C.; MacDiarmid, A. G. *Syn. Metals* **1986**, 13, 193

(36) Tan, K. L.; Tan, B. T. G. *J. Chem. Phys*. **1991**, 94, 15

(37) Golczak, S.; Kanciurzewska A.; Fahlman, M.; Langer, K.; Langer, J. J. *Solid State Ionics* **2008**, 179, 2234

(38) Park, J. H.; Kim, J. S.; Lee, J. H.; Lee, W. H.; Cho, K. *J. Phys. Chem. C* **2009**, 113, 17579

(39) Shieh, J. T.; Liu, C. H.; Meng, H. F.; Tseng, S. R.; Chao Y. C.; Horng, S. F. *J. Appl. Phys.* **2010**, 107, 084503

(40) Stylianakis M. M.; Kymakis, E. *Appl. Phys. Lett.* **2012**, 100, 093301

(41) Shrotriya, V.; Wu, E. H. E.; Li, G.; Yao, Y.; Yang, Y. *Appl. Phys. Lett.* **2006**, 88, 064104

(42) Kymakis, E.; Servati, P.; Tzanetakis, P.; Koudoumas, E.; Kornilios, N.; Rompogiannakis, I.; Franghiadakis, Y.; Amaraunga, G. A. J. *Nanotechnology*, **2007**, 18, 435702

초 록

본 연구에서는 기존의 유기태양전지의 정공 수송 층으로 쓰였던 PEDOT:PSS 의 단점인 산성인 환경과 낮은 전기전도도를 보완하고 향상시키기 위해 poly(styrene sulfonate) 사슬에 polyaniline을 grafting 시켜 향상된 전기 전도도를 보이는 PSSA–*g*–PANI 을 합성하였고 이를 더욱 향상시키기 위해서 산화 그래핀인 graphene oxide (GO)을 첨가하여 PSSA–*g*–PANI/GO 복합체를 만들고 이를 유기태양전지에 정공 수송 층으로 적용시킨 연구이다. PSSA–*g*–PANI/GO 복합체는 PSSA–*g*–PANI 대비 GO의 무게를 달리하면서 합성하였다. 이 복합체의 특성은 UV-Vis spectroscopy를 통해 복합체 필름의 투명도를 측정하였고, cyclic voltammetry를 통해 각 복합체들의 the highest occupied molecular orbital (HOMO) 에너지 준위를 측정하여 유기태양전지의 정공 수송 층으로써 적용이 가능한지 알아보았다. 복합체의 투명도는 GO의 무게비가 PSSA–*g*–PANI 대비 5 wt% 인 복합체까지 PEDOT:PSS보다 높은 투명도를 보였으나, GO가 많이 들어갈수록 낮은 투명도를 보였다. HOMO 에너지 준위를 각 복합체 모두 4.8 ~ 4.9 eV 값이 나와서 정공 수송 층으로써 적용이 가능했다. 그리고 GO를 첨가한 복합체의 경우 GO의 카르복실산 작용기 때문에 polyaniline이 proton doping 되어서 더 높은 전기전도도를 보였지만, GO가 많이 들어갈수록 GO의 절연체 역할로 인해

전기전도도가 낮아지는 경향을 보였다. GO의 doping 효과는 X-ray photoelectron spectroscopy를 통해 확인하였다.

최종적으로 이를 유기태양전지의 정공 수송 층으로 적용시켰을 때 PSSA–*g*–PANI/GO(2.5) 에서 가장 높은 효율인 4.23 %를 나타냈고 이는 기존 물질인 PEDOT:PSS 보다 23% 향상된 효율을 나타냈다. 이와 같은 효율 향상은 단락전류밀도와 충전률의 향상에 의해 나타난 결과이다. 이를 확인하기 위해 External quantum efficiency (EQE)를 측정한 결과, 효율과 같은 경향으로 단락전류밀도가 나왔고 충전률의 경우에는 직렬저항과 분로저항를 구해 충전률 향상 이유를 확인하였다. 또한 정공 수송 층에 따른 소자의 정공 이동도를 측정한 결과, 효율과 같은 경향성을 나타냈다.

결론적으로 이 연구에서는 기존 정공 수송 층 물질인 PEDOT:PSS 대비 투명도와 전기전도도를 향상시킨 PSSA–*g*–PANI/GO 복합체를 만들어 유기태양전지에 적용시킴으로써 4.23% 라는 기존 물질 대비 23% 향상된 효율을 보고했다.

주요어: graphene oxide, PSSA–*g*–PANI, 정공 수송 층, 유기태양전지
학 번: 2012-20602